Progress in PHOTOVOLTAICS

PROGRESS IN PHOTOVOLTAICS: RESEARCH AND APPLICATIONS
Prog. Photovolt: Res. Appl. (2012)
Published online in Wiley Online Library (wileyonlinelibrary.com). DOI: 10.1002/pip.2302

RESEARCH ARTICLE

Empirical assessment of short-term variability from utility-scale solar PV plants

Rob van Haaren[1]*, Mahesh Morjaria[2] and Vasilis Fthenakis[1]

[1] Center for Life Cycle Analysis, Department of Earth and Environmental Engineering, Columbia University, 500 West 120th Street, New York, NY 10027, USA
[2] First Solar, Inc., 350 West Washington Street, Suite 600, Tempe, AZ 85281, USA

ABSTRACT

Variability of solar power is a key driver in increasing the cost of integrating solar power into the electric grid because additional system resources are required to maintain the grid's reliability. In this study, we characterize the variability in power output of six photovoltaic plants in the USA and Canada with a total installed capacity of 195 MW (AC); it is based on minute-averaged data from each plant and the output from 390 inverters. We use a simple metric, "daily aggregate ramp rate" to quantify, categorize, and compare daily variability across these multiple sites. With this metric, the effect of geographic dispersion is observed, while controlling for climatic differences across the plants. Additionally, we characterized variability due to geographical dispersion by simulating a step by step increase of the plant size at the same location. We observed maximum ramp rates for 5, 21, 48, and 80 MW_{AC} plants, respectively, as 0.7, 0.58, 0.53, and 0.43 times the plant's capacity. Copyright © 2012 John Wiley & Sons, Ltd.

KEYWORDS

short-term variability; PV plant ramp rate; daily aggregate ramp rate; inverter shells

***Correspondence**

Rob van Haaren, Center for Life Cycle Analysis, Department of Earth and Environment Engineering, Columbia University, 500 West 120th Street, New York, NY 10027, USA.
E-mail: rv2216@columbia.edu, Rob.vanHaaren@firstsolar.com

Received 21 December 2011; Revised 19 June 2012; Accepted 8 September 2012

1. INTRODUCTION

A major challenge in integrating high penetrations (>20%) of solar and wind energy rests in the grid's ability to cope with the intrinsic variability of these renewable resources. Germany and Denmark, respectively, already generate 9% and 22% of their electricity from wind and solar power and have found means to address these challenges, viz. by relying on strong grid interconnections with other countries and flexible thermo-electric generators to provide backup when necessary [1,2]. Although such high levels of penetration may be a decade or two away in most other operating regions, we must find measures to manage variability, especially when such mitigation approaches are unavailable or ineffective. Further, besides assuring reliability, effective integration of high levels of solar and wind power can reduce the "hidden" costs and emissions associated with larger than necessary backup capacity.

A mechanism of markets operating on different timescales maintains the balance between supply and demand in most electricity grid systems. First, there is the day-ahead market, wherein hour-by-hour generation is scheduled on the basis of load forecasts for the next day. Then, there is the real-time market that, in the New York Independent System Operator, opens 75 min before the operating hour and serves to balance the latest intra-hour load forecasts (typically 15 min). These two comprise the so-called "energy markets." To maintain reliability of the grid, additional markets exist to deal with short-term fluctuations that the energy markets do not capture, such as the demand response and ancillary services markets. The ancillary services, in turn, consist of "reserves" and "regulation," where the spinning and non-spinning "reserves" accommodate unexpected outages of lines or generators (contingencies), whereas "regulation" manages short-term variability in demand and supply.

Variability of solar resources is subdivided in long-term and short-term fluctuations. Studies of the former focus on the diurnal cycle and the required portfolio of generators in the grid (typically with hourly data). Previous researches assessed the renewable penetration limits of current grid systems [3–6] and scenarios with energy storage [7].

Short-term variability studies use second-to-minute averaged data to investigate the effect on operating reserves and frequency regulation. When the short-term variability of solar and wind power is no longer masked by the load variability, grid operators must increase system operating reserves and regulation services to maintain the grid's reliability. This approach, in turn, raises the operating costs associated with integrating photovoltaic (PV) renewable energy into the grid. The actual increase in cost depends upon various factors, including the grid's size and inherent flexibility, and the aggregated variation of all the renewable energy in a grid-balancing area (General Electric, 2010).

With the projection of large-scale PV plants (>250 MW) becoming significant generators on the grid in the near future, system operators started discussions on how to deal with the plant's inherent variability. The backbone of these discussions is based on assessments of plant variability gleaned from irradiance sensors data or relatively small (~5 MW) existing plants. Extrapolating these point source data to multi-megawatt plants may not be valid because the effect of geographic dispersion from large scale plants is not completely understood yet. Because of the potential impact of the uncertainty arising from these studies, it is important to analyze the ramp rates recorded from operating multi-megawatt plants and compare them with published findings.

To what extent renewable electricity sources will affect the grid is restrained by their inherent variability and the extent to which their output can be forecasted. Low short-term variability and high predictability of ramps are desirable for minimizing the extent of regulation and the amount of reserves required.

In scenarios of high solar and wind penetration on the grid, generation-side variability is expected to dominate the load variability and drive the need for higher level of regulation. Forecasting can play a crucial role here; expected ramps can be dealt with by controlling the dispatch of conventional generators. Several vendors utilize weather models to develop 1–48 h forecasts for PV plants on varying time-averaging periods with sufficient accuracy to aid grid operators in maintaining reliability. However, short-term cloud-driven changes in solar plant output (tens of seconds to minutes) are hard to forecast. As more renewables become part of the generator portfolio, characterizing variability and forecasting will become key components of balancing of supply and demand of power on the grid. In this study, we start with the characterization of solar plant output variability which is a contributor to the aggregated output variability of all plants in a balancing area. It will then be followed by a forecasting and power flow analysis study.

A central term in this study is the "ramp rate" ($RR_{\Delta t}$), defined herein as the change in power output of a PV plant or irradiance sensor over two consecutive periods of the duration Δt. In this study, we use power outputs (or irradiance values) that are averaged over 1 min. We also use 1 min as the time interval (Δt) for ramp rate calculations. The units used for the *RR* are on a per-unit basis, that is, 1 p.u. = rated plant AC capacity and for irradiance sensors 1 p.u. = 1000 W/m^2.

2. PREVIOUS STUDIES ON SOLAR VARIABILITY

The short-term variability of solar power has recently garnered much attention because the installed capacity is increasing very rapidly, and the technology is on its way to become a significant part of the generator portfolio (power capacity) of several countries, notably Germany (12%, 2010), and Spain (4.3%, 2010) [2,8]. Fine time-resolution data are needed for these studies because hour-by-hour data do not capture such variability [9]. Early studies relied on irradiance measurements [10,11], converting them to clearness indexes as a universal indicator. This index embodies the quotient between global horizontal irradiation at ground level (GHI_{ground}) and the extraterrestrial irradiation (GHI_{et}).

There are many ways in which variability of power output can be characterized. A common approach is to use the standard deviation of power output (or clear sky index) changes for a certain averaging interval over a period of time, as described in [12]. The highest ramps are sometimes described by looking at the 99.7th percentile value, which is, in a normal distribution, three standard deviations from the mean (3σ). Mills *et al*. found the 1 min standard deviation and 99.7th percentile values to decrease from, respectively, 0.08 and 0.58 for a single site, to 0.02 and 0.09 for all 23 sites studied (20–440 km apart).

More recently, output variability was derived from satellite imagery by Hoff and Perez, allowing the collection of high-frequency data for a large number of points on the map [13]. Although the Perez model is bound by its one-dimensionality and its inability to deal with evolving cloud fields, it gives a useful relationship between the "zero-correlation crossover distance" and the sampling interval for short-term variability.

Previous studies have shown that geographical smoothing already occurs when comparing an irradiance sensor's ramps with those of a small 30 kW plant [14]. This is in line with findings from Mills *et al*. and Perez *et al*. where the correlation of irradiation at pairs of sites was found to decrease with distance. Some studies that employ irradiance ramps as a proxy for plant output ramps disregard the fact that many utility-scale PV plants have inverters with limited capacity, limiting the PV power they can feed to the grid. For example, if irradiance reaches above clear-sky levels because of reflection from clouds, it is included as a ramp rate, whereas the actual inverter's output may not exceed its own power limit. Also, irradiance sensors do not capture the influence of the modules' temperature and spectral response on power output unless special adjustments are factored in.

Observed or modeled ramp rates from published studies on variability using multiple data points or single large-scale plants are summarized in Table I. Five of these nine studies looked at the variability of operating PV plants. Wiemken *et al*. assessed the 5 min-averaged output changes of 100 PV systems across Germany (600×750 km^2) [15]. Hansen investigated the variability of a single 4.6 MW utility-scale plant in Springerville, AZ, on timescales of 60, 15, 4, and 1 min, and

DOI: 10.1002/pip

Table I. Data types of published variability studies and the observed extreme ramp rate for all data points.

Study	Data type	Data points	Time scale (smallest)	Distance (km)	Observed extreme ramp rate (p.u.)
[15]	PV systems (1–5 kW)	100	5 min	Few–750	0.05
[27]	Irradiance	9	1 min	1.3–5	0.212
[17]	PV systems: 121–228.5 kW (part A) and 4.6 MW (part B)	3 trackers (A) and 1 fixed (B)	Part A: 10 min; part B: 10 s	110–280	Part A: 0.41 per 10 min; part B: ~0.50 (1 min data)
[23]	PV systems (0.12–5.6 kW) and irradiance	52	1 min	Few–1000	—
[18]	PV system (25 MW)	6 blocks (trackers)	10 s	—	0.2
[12]	Irradiance	23	1 min	20–440	0.2
[28]	Irradiance	4	1 min	19–197	0.12 (based on 5 min data)
[16]	PV system (4.6 MW)	1	10 s	—	~0.50 (1 min data)
[22]	Irradiance and satellite (virtual networks)	24	20 s	—	—
[19]	PV system (13.2 MW)	1 (tracker)	1 s	—	0.50 (1 min data)

One-minute-averaged data are used, unless otherwise noted. Ramp rates for irradiance data are denoted as fraction of 1 sun (1000 W/m^2 = 1 p.u.).

10 s [16]. A "cloudy" winter day was chosen to analyze fluctuations in output, resulting in ramp rates of up to 0.46, 0.3, 0.5, 0.45, and 0.3 p.u., respectively.

At the time of writing, four publications included output data from multi-megawatt systems: two reported on the 4.6 MW Springerville PV plant [17,16], one on a 25 MW tracker plant in Florida [18], and one on a 13.2 MW tracker plant in Nevada [19].

Our study is based on data from six utility-scale PV plants with an AC capacity between 5 and 80 MW, located in the southwest of the USA and southeast of Canada (Table II). These plants utilize First Solar's CdTe thin-film modules and BOS Technologies. The goal of this study is to identify a way to estimate the variability of planned projects (even beyond 80 MW) and present this to the independent system operators. To determine what characterization of variability in generator output is most useful for independent system operators, we interviewed a renewable integration specialist at the California Independent System Operator [20]. He agreed that a variability classification of days would be useful in projecting what effect a planned project will have on balancing of supply and demand on the grid. In this study, we propose a method to do this.

Table II. Overview of sources of photovoltaic plant data used in this study.

AC capacity [MW]	State	Country	No. of days in data
80	South Ontario	Canada	560
48	South Nevada	USA	369
30.24	North New Mexico	USA	233
21	Southeast California	USA	537
10	South Nevada	USA	547
5	South Ontario	Canada	200

3. DAILY AGGREGATE RAMP RATE

In previous publications [16,21,12,22], researchers quantified variability using different methods for single days, qualitatively denoting them as, for example, *a very cloudy day* or *a highly variable day*. The expected ramp rates from a normally operating utility-scale PV plant are a function of timescale, time of day, the plant's shape and size as well as cloud coverage and movement. To account for impact of cloud coverage and movement, we present a quantitative metric called the daily aggregate ramp rate (DARR) to characterize daily variability in a utility-scale plant. This metric can be used to compare observed ramp rates from plants in different locations and of different sizes by selecting days with similar DARR values.

A DARR allowing the categorization of days based on the observed minute-averaged variability is defined as

$$DARR_{\min} = \sum_{t=1}^{1440} \frac{|I_t - I_{t-1}|}{C}$$

with I_t being the minute-averaged irradiance (W/m^2) of a single plane of array (POA) irradiance sensor at time t, and C the constant equal to 1 sun (1000 W/m^2). A single irradiance sensor is chosen for this metric rather than the plant's output so that the plant's size and shape does not influence the $DARR_{\min}$.

On a perfectly clear sky day, one can expect a $DARR_{\min}$ of ~2 p.u., that is, the irradiance climbs to ~1000 W/m^2 at solar noon and then drops back to 0 W/m^2 in the evening. The most extreme days show a $DARR_{\min}$ of 70–80 p.u. Days were classified into five categories, ranging from very stable days (Category 1) to highly variable ones (Category 5).

- Category 1: $DARR_{\min} < 3$
- Category 2: $3 \le DARR_{\min} < 13$
- Category 3: $13 \le DARR_{\min} < 23$
- Category 4: $23 \le DARR_{\min} < 33$
- Category 5: $33 \le DARR_{\min}$

The categories are somewhat arbitrary but are expected to be representative. The DARR metric has limitations regarding the fact that peak clear-sky irradiance values vary throughout the year, as well as the length of day (winter days have lower clear-sky peak POA irradiance and are shorter than summer days). Because of this, the first DARR category was set to include days with *DARR* 3 instead of $DARR < 2$. Figure 1 illustrates a Category 1 day and Category 5 day.

We note that completely overcast days show very small ramps (sometimes $DARR_{min} < 1$), so, like days with a clear sky, they fall under Category 1. To account for overcast days, a special sub-category was created and presented in the results.

The distribution of days over $DARR_{min}$ categories indicates the variability observed at a specific location. Depending on the size of a planned project, this information would be helpful for grid operators in assessing the system reserves required on the grid. A closer look at fluctuations in plant output for each $DARR_{min}$ category is given, thereby providing insight into the anticipated ramp rates from plants of different sizes.

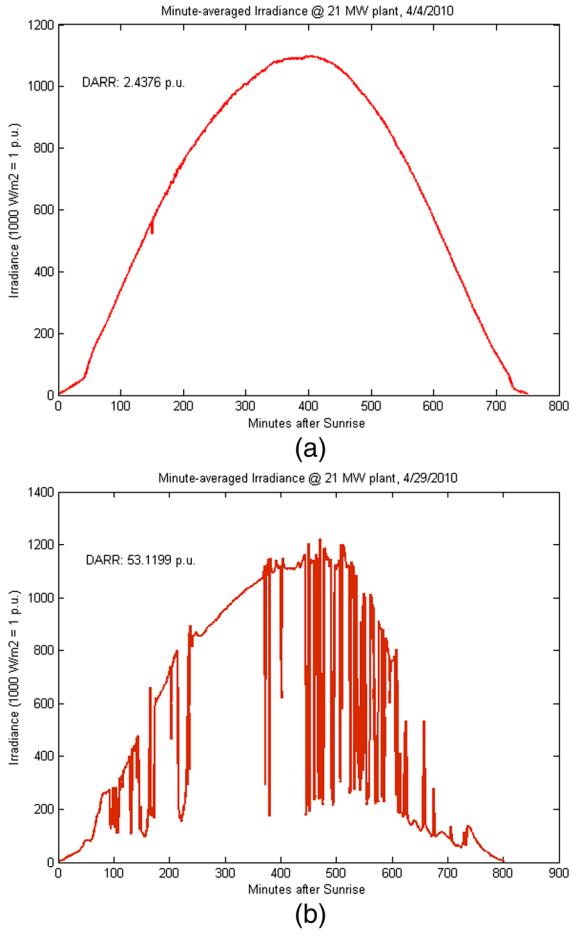

Figure 1. Minute-averaged irradiance sensor measurements at the 21 MW plant in California for (a) a "Category 1" day and (b) a "Category 5" day, both in April 2011. The $DARR_{min}$ is 2.4 and 53.1 p.u., respectively.

We note that because this metric summarizes ramp rates for a whole day, the character of individual 1 min ramps is lost. Thus, when we consider two dips in irradiance measurements of the same magnitude (A and B), they can contribute the same amount to the $DARR_{min}$, but dip A could be much steeper than dip B (for instance, because of a higher cloud velocity). Also, because the DARR is based on a minute-by-minute basis, it does not capture higher frequency events.

4. RAMP RATES AND GEOGRAPHIC DISPERSION

In studying the effect of PV systems on the grid, we must consider variability in the output of all grid-connected PV systems located in a system operator's service area. Several studies have detailed the effect of geographic dispersion on the output variability of many smaller systems or irradiance sensors. Thus, Wiemken *et al*. found that the highest 5 min ramp rate for a single system was 52% of system capacity, whereas 100 systems, together totaling 243 kW, showed ramp rates up to only 5% of the total capacity [15]. Murata *et al*. [23] introduced the term "output fluctuation coefficients": the ratio between the maximum observed ramp rate in a certain time window, over the standard deviation of ramp rates in that same time window. As the number of systems increases, the coefficient reaches an asymptote depending on the width of the time window and the season. Besides that, pair-wise correlations of PV system ramp rates were derived from the data; they were shown to be close to zero, even for distances around 50 km. In fact, 1 min ramp rate correlations already had declined to 0.12 for two inverters within a single plant [21]. As ramp rate correlations on a per-minute basis drop significantly over sub-kilometer distances [21], multi-megawatt PV systems also exhibit some degree of geographic dispersion. In fact, when plants extend beyond the size of fast-moving cumulus clouds, variability is reduced as the clouds cover only part of the array. Another effect is that clouds often do not move fast enough to completely cover a plant from one time interval to the next, as we will discuss later in this section. With a 290 and 500 MW plant under construction, it is important to assess what variability can be expected from them. Other multi-megawatt plants were shown to exhibit extreme (minute) ramp rates of up to 50% for a 4.6 MW system [16] and 45% for a 13.2 MW system on a "highly variable day" [21]. Kankiewicz *et al*. [18] assessed variations in the output of a 25 MW two-axis tracker system in Florida, recording minute-averaged ramp rates of up to ~20% during a single day's output. Of course, comparing these PV plants is questionable because the systems differ in shape, size, and panel orientation. Furthermore, the clouds' shape, size, and velocity are not specified, so climatic conditions cannot be compared; nevertheless, the trend clearly suggests that their size is important.

Hoff and Perez introduced the term "dispersion factor" (D), a dimensionless variable capturing the relationship between PV fleet length (L), cloud velocity (V), and the used time interval (Δt). It is defined as the number of time intervals needed for a cloud to pass over the entire PV fleet in excess of unity [13].

$$D = 1 + \frac{L}{V\Delta t}$$

Three regions of geographic density were defined (crowded, limited, and spacious) and one optimal point, where D equals the number of systems (N) in the fleet. An example is presented to validate the model for the Springerville plant, where Hansen [16] observed a 50% one-minute ramp rate. Assuming a size of 420 m by 420 m for the 4.6 MW plant ($L = 420$ m) and $\Delta t = 60$ s, the authors concluded that with an average wind speed of 3.5 m/s (D becomes 3), the observed relative output variability would be 60%. However, extreme ramp rates typically are known to occur with high cloud velocities (>20 m/s). If a modest value of 7 m/s was used for their data validation, the model would predict a relative output variability of ~80% for this plant.

A simple estimate of extreme ramp rates for a single plant with capacity P_{cap} is made by looking at how much the plant's time-averaged output $\bar{P}_{\Delta t}$ is reduced from being completely unshaded to being (partly) shaded. For rectangular-shaped plants, the highest ramp rates can be expected when a hypothetical cloud, bigger than the array itself, is moving in the direction parallel to the shortest side, L of the plant [meters], with a velocity V in m/s. The power output $P(t)$ will change linearly, with a slope P [MW/s]:

$$\bar{P} = -P_{cap}\frac{(p_{clear} - p_{shade})V}{L}$$

where p_{clear} and p_{shade} are the per-unit power outputs under zero-shading and fully shaded-conditions (typically 1 and ~0.15, respectively, depending on spectral response of modules). The power output will continue to drop until the whole array is shaded ($P(t) = P_{cap} - p_{shade}$), yielding the following equation:

$$P(t) = P_{cap} - \max\left(p_{shade}, p_{clear} - \frac{(p_{clear} - p_{shade})V}{L}t\right)$$

We note that for events with $L/V > \Delta t$, the cloud cannot cover the whole array within a single time interval, thus the per-unit ramp rate is less than avg(p_{clear}, p_{shade}). Averaging the power output over time interval Δt, we obtain extreme ramp rates $RR_{\Delta t,max}$ [MW]:

$$RR_{\Delta t,\max} = P_{cap} - p_{clear} - \bar{P}_{\Delta t}$$

with,

$$\bar{P}_{\Delta t} = \frac{\sum_{t=1}^{\Delta t} P(t)}{\Delta t}$$

For $L/V > \Delta t$, the average power output is equal to $P(\Delta t/2)$ and the maximum per-unit ramp rate becomes

$$\frac{RR_{\Delta t,\max}}{P_{cap}} = \frac{(p_{clear} - p_{shade})V}{2L}\Delta t$$

Figure 2 and throughout the rest of the paper, $RR_{\Delta t,\max}$ is plotted on a per-unit basis with time interval $\Delta t = 60$ s,

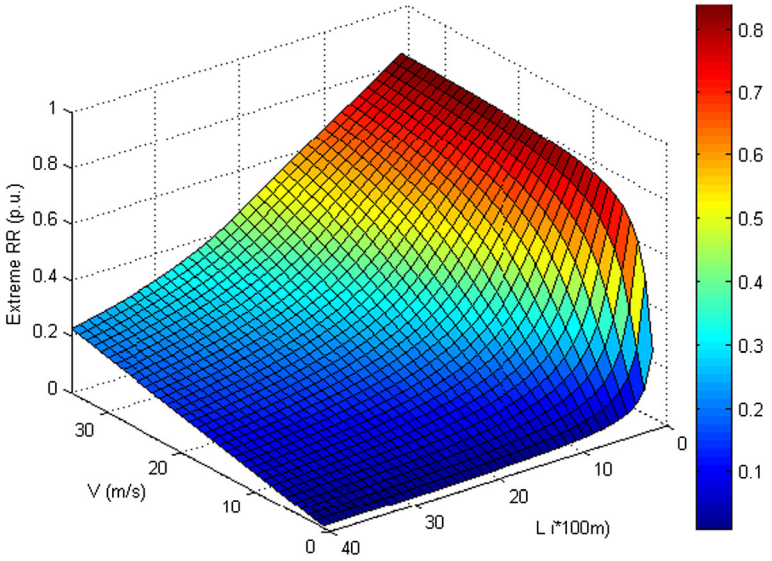

Figure 2. Extreme ramp rate (RR) as a function of cloud velocity (V) and the shortest side of plant (L) for a hypothetical cloud moving over the array in direction parallel to L. Parameters *pclear* and *pshade*, respectively, are set to 1 and 0.15, and the interval over which power is averaged is 60 s.

as a function of V and L. The parameters p_{clear} and p_{shade}, respectively, are set to 1 and 0.15, on the basis of observed plant outputs under those conditions. Smaller plants ($L < 500\ \boldsymbol{m}$) already show a steep increase of $RR_{\Delta t,max}$ at small cloud velocities, whereas for plants with shortest side $L > 60V$, the graph depicts a more linear dependency on V, with its slope decreasing as L increases. For the 80 MW_{AC} plant, which measures approximately 2000 m by 2200 m, cloud velocities of 30 m/s may yield ramp rates of up to 0.4 p.u. or 32 MW.

The upper boundary of V is chosen based on the cloud speeds of 95 km/h (26.4 m/s) that were reported by Perez *et al*. for a single day in the atmosphere radiation measurement network [22] and from cloud velocities reported by others [24]. We hypothesized that the ramp rates from the simple model overestimate the observed ramp rates because of the following shortcomings.

First, complete shading of arrays with $L > 3500$ m by a single cumulus is rare because single cumuli become less common with increasing size [25]. In addition, the model assumes that the incoming cloud has a perfectly flat front and uniform obliqueness, exerting the highest possible ramp rate at the prevailing cloud velocity, although such clouds are unlikely to occur for high values of L. Also, in measuring plant output, we must consider that there is a probability related to the location of a cloud shadow at the beginning of an interval. Finally, shortcomings exist in the model related to plant morphology and prevailing wind directions, as it cannot assess other shapes of PV plants besides rectangular ones. Accordingly, the ramp rates illustrated in Figure 2 are likely to overestimate those actually observed. We are now refining this model by including distributions of cloud size and accounting for different shapes of plants.

Because plants are of multi-megawatt size and are constructed with a uniform megawatt-array approach as discussed in the succeeding section, it is possible to describe the effect of geographic dispersion at a single site for different sized plants. Similar to Kankiewicz *et al.* [18] and Lenox [19], where variability was described for a stepwise increasing amount of capacity, our study follows an approach called the "inverter shells method", wherein variability is described with an increasing number of 0.5 MW inverters. We delineate this method in Section 7.2.

5. DATA

Data were collected for six multi-megawatt First Solar PV plants, four of which are located in the US southwest and two in Ontario, Canada. We collected minute-averaged power plant output, single inverter output, and data from weather stations (with GHI and POA irradiance sensors).

Construction of these plants covers multiple phases, in which blocks of power come online as they are completed. Total capacity therefore is built up in steps until the whole plant is completed. Unfortunately, not all plants were online for a full year at the moment of data collection. However, the first half of 2011 (1 January– 30 June) sketches a good comparative picture of plant variability at different sites.

Plant output data are stored in units of kilowatt from one or more energy meters per plant. Other plant data include data from weather stations that provide ambient temperature, barometric pressure, wind speed/direction, precipitation, and GHI and POA irradiance in watts per square meter (±2%).

Besides the complete plant outputs, data were collected at the inverter level (~0.5 MW_{AC} units) allowing us to model sub-plant output, as we show later in the *inverter shells method*. The plant structure is as follows: a plant consists of multiple power conversion stations located in the center of PV arrays of about 1.2 MW_{DC}. A power conversion station consists of two ~500 kW_{AC} inverters that feed a single transformer. Each inverter is connected to four combiner boxes that congregate currents from 14 harnesses. In turn, each harness comprises 15 strings of 10 modules. The dimension of the sub-array connected to a single inverter is typically 50 m latitudinally by 250 m longitudinally (Figure 3).

6. METHODOLOGY

As a first step, we employed minute-by-minute POA irradiance data from a central weather station to calculate the DARR values for each plant day. We excluded days with data errors from the categorization to prevent them from skewing the distribution. In the following, the assessment of plant output variability is outlined.

6.1. Plant output variability

The data were processed in MATLAB (version 7.11.0) using a modular approach, as summarized in the flowchart (Figure 4).

First, the data were checked for consistency and completeness, and the days with data errors were flagged during the data validation process. The next module was to create cumulative distribution functions (CDFs) and histograms of ramp rates for a selected plant-month, including the DARR averages to indicate variability in that month. Then, times when power output >0 kW were defined as daytime. Finally, the ramp rates of these output values were calculated and normalized with plant capacity. Finally, the results were plotted in logarithmic-scale histograms and cumulative distribution functions.

6.2. Inverter shells method

An "inverter shells method" is introduced to investigate reduction in variability due to geographical dispersion with increasing plant sizes. This method has an advantage over studying ramp rates from different sized plants located in completely different areas because weather conditions within the same plant will be the same (as will be the modules, inverters, and transformers).

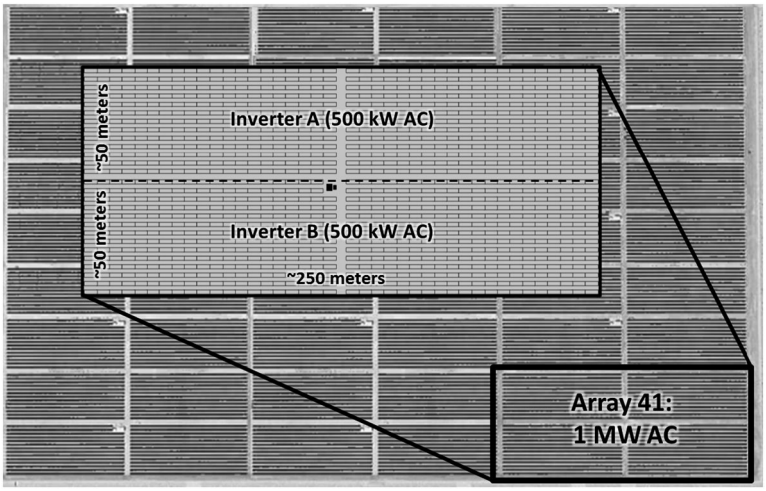

Figure 3. Outline of the 1 MW (AC) arrays at the 48 MW PV plant. The inverters are the lowest level at which data are collected.

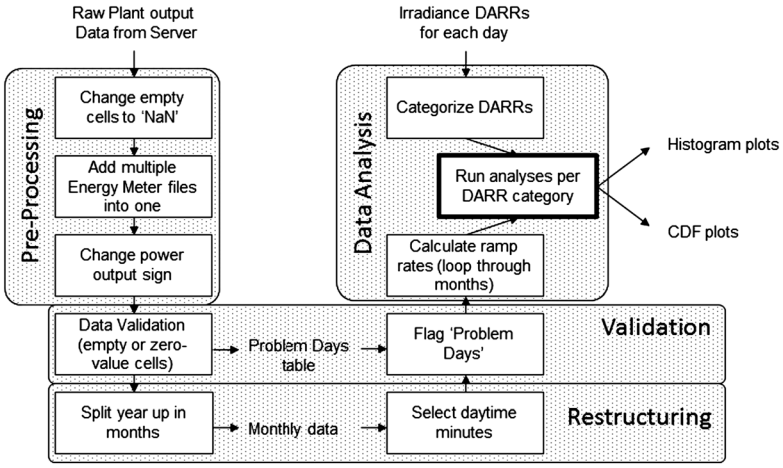

Figure 4. Schematic overview of data processing, starting with raw output from the plant and irradiance measurements from the central data server. The results are depicted as histogram plots and cumulative distribution functions (CDFs).

Starting with the output profile of an array connected to a single inverter (0.5 MW), shells of inverters are added in each step, resulting in multiple CDFs (Figure 5). We kept the aspect ratio of each of the "sub-plants" the same (1:5), thereby counteracting the effect on ramp rates from a prevailing wind direction.

In the 48 MW plant, eight steps were performed in this fashion, with the last step counting eight by eight arrays with 0.5 MW_{AC} inverters, that is, a capacity of 32 MW_{AC}.

7. RESULTS

7.1. Daily aggregate ramp rate

Using the five DARR categories introduced in Section 4, we characterized the variability at each plant. Table III details the resulting distribution, with incomplete data sets denoted with "(i)". It reveals that the irradiance ramp rates differ with the prevailing climate at each location. The 21-MW plant showed 49% "Category 1" days in 2011. The 80 MW and 5 MW plant located in Ontario, Canada, showed only 16 and 17% of low variability days. However, only about a quarter of those "Category 1" days indeed were clear sky days, whereas the rest was overcast.

It should be noted that the irradiance database for the 30.24 MW plant was not complete in April and June 2011. This likely resulted in fewer clear sky Category 1 days than actually occurred.

7.2. Irradiance sensors versus plant output

Many studies employed irradiance-sensor data as a proxy for plant output (Table I). However, this method is not yet validated with measured plant data. With First Solar's original data, we investigated how ramp rates observed

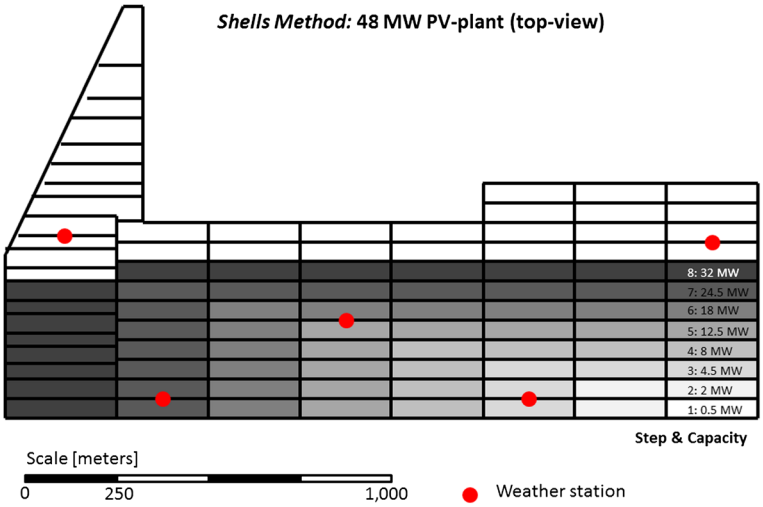

Figure 5. Top view of the 48 MW_{AC} plant. Every rectangle represents an array connected to a single inverter (0.5 MW_{AC}). The shells method is outlined starting from step 1 in the bottom-right corner. With every step, variability is characterized as the plant grows bigger. Red dots represent weather stations where irradiance sensors are located.

Table III. Daily aggregate ramp rate category distribution for a single irradiance sensor in all photovoltaic plants studied.

Year:	2010					2011 (i)					
Capacity (MW_{AC})	21	30.24 (i)	48 (i)	10	80 (i)	21	30.24	48	10	80	5
Category 1 clear sky (%)	41	19	43	32	4	49	16	34	33	4	4
Category 1 overcast (%)	1	1	2	2	10	0	0	1	1	12	12
Category 2 (%)	29	39	20	28	33	21	34	24	24	37	39
Category 3 (%)	16	28	19	19	19	16	23	17	17	20	20
Category 4 (%)	7	4	9	10	14	10	13	12	13	13	10
Category 5 (%)	7	7	8	8	20	4	14	11	13	14	16
No. of days	336	67	176	349	358	201	166	193	198	202	200

All the data are expressed as per cent of total number of days with clean data (percentages may not total 100 due to rounding). The bottom row displays the number of days with clean data for these locations.

from single and dispersed irradiance sensors at POA compare with the plant's ramp rates. In Figure 6, we display the per-unit output of these sources for a 35 min time span at the 48 MW facility on 19 May 2011 (the red dots in Figure 5 show the locations of the five irradiance sensors within the plant).

The per-unit output of five irradiance sensors aggregated is a much better indicator of the overall plant output than that of a single sensor, even though the values above and close to 1 p.u. deviate more from plant output. As we introduced earlier, this happens because the AC output capacity of the inverters is limited and a momentary higher irradiance does not result in higher AC output. Accordingly, it is appropriate to clip irradiance of each sensor to 1000 W/m^2 if that level is surpassed.

Figure 7 illustrates the improvement by using "clipped" irradiance data, where we compare the output data for the 48 MW plant for January–June 2011 with a single irradiance sensor, five sensors aggregated, and five sensors aggregated after they were clipped individually. Overall, the unclipped data overestimate the plant's highest ramps by 5–10% whereas the clipped version approximates within a 3% error.

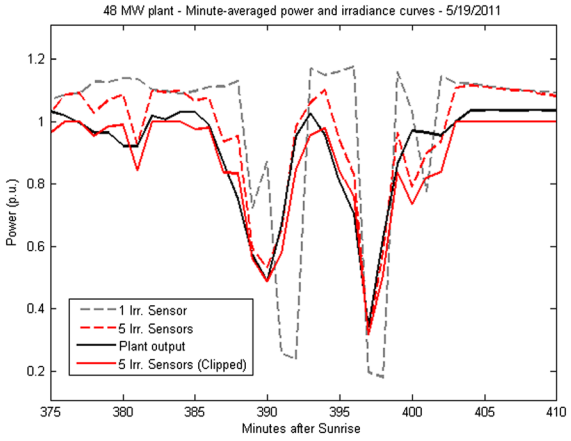

Figure 6. Plant output (1 p.u. = 48 MW_{AC}) compared with the output of a single irradiance sensor, five aggregated sensors, and five aggregated sensors "clipped" down to 1000 W/m2. The "smoothing effect" of adding more sensors is apparent as the plant's output curve is approached. However, it also shows that both the single and aggregated irradiance sensor curves overestimate the plant's peak output.

7.3. Inverter shells method

Figure 8 displays how variability declines as an increasingly bigger sub-plant at the 48 MW plant is monitored. In eight steps, the sub-plant's output is increased from 0.5 to 32 MW_{AC} using the inverter shells method introduced earlier.

As the plant grew from 0.5 to 32 MW, the standard deviation of daytime 1 min ramps decreased from 0.059 to 0.032 p.u. This drop is not as significant as observed in Mills *et al*., where the standard deviation decreased from 0.08 to 0.02 p.u. when variability from one site was compared with that of 23 sites. This is expected, because the distance between sites in the latter study is much bigger than the distances between inverters in the single plant studied here. The observed maximum ramp rate fell from 0.87 to 0.67 p.u., whereas $RR_{60s,3\sigma}$, that is, at 0.997 probability dropped from 0.56 to 0.24 p.u. This ramp rate reduction observed within a single PV plant is in line with findings from previous studies [26,21]. The lower reduction in $RR_{60s,max}$ compared with $RR_{60s,3\sigma}$ reflects the effect of the occurrence of cloud velocity and its influence on ramp rates of different sized plants, as shown in Figure 2. We note, however, that a cloud velocity of 7 m/s already suffices to cover the plant with $L = 400$ m in the last step (32 MW). In the future, we will be able to apply this technique to bigger plants and obtain a better idea of how extreme ramps are reduced beyond $L = V\Delta t$.

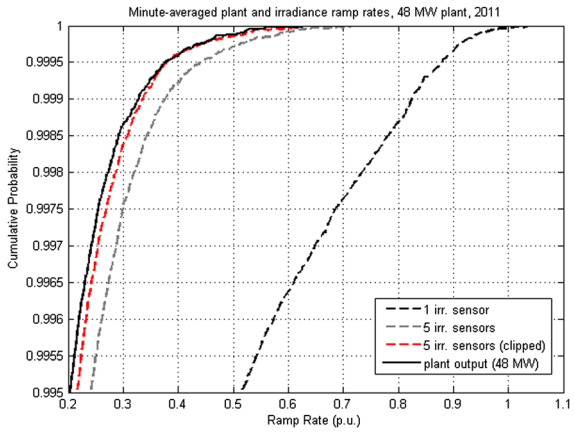

Figure 7. Cumulative probability distribution showing the highest 0.5% ramp rates observed from the whole plant (48 MW_{AC}), a single irradiance sensor, five sensors, and the five sensors clipped down to 1000 W/m^2 for all daytime data of January–June 2011.

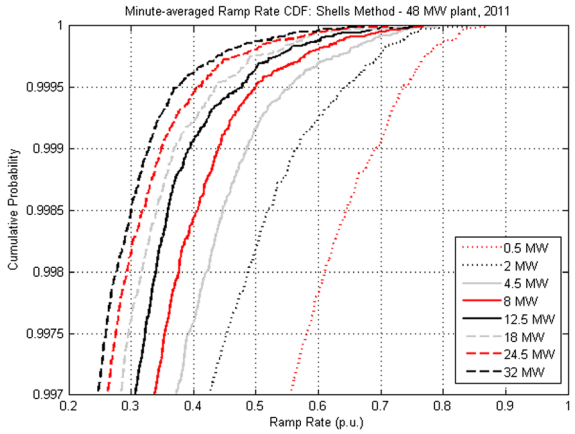

Figure 8. Cumulative probability curve showing the effect of plant size on observed extreme ramp rates as a fraction of plant capacity. Results are obtained from applying the inverter shells method to the 48 MW plant, using data from January to June 2011.

7.4. Observed plant ramp rates

The common practice for showing the magnitude of ramp rates is by plotting histograms or CDFs of absolute values. Figure 9 shows a histogram of daytime ramp rates observed at the 5 and 80 MW plants. Both are located in the same area of Ontario, Canada, so weather difference effects are expected to be minimal. The 80 MW plant exhibits relatively less variation compared with the 5 MW plant. Because of symmetry observed in histograms, it is suitable to use CDF curves for displaying ramp rates; the latter approach will be used throughout the rest of this paper.

Some second-by-second data were made available for the 5 and 80 MW plants, and Figure 10 gives an overview of the observed power output ramps from these plants in daytime of May 2011. The second-by-second data show lower relative ramps compared with minute data, as was concluded by previous studies [19,21].

After the DARR categories were defined, plant ramp rates were analyzed for each separate category. Figure 11 shows the occurrence of ramp rates for each category at the 80 MW plant in 2011; the highest ramp rate observed

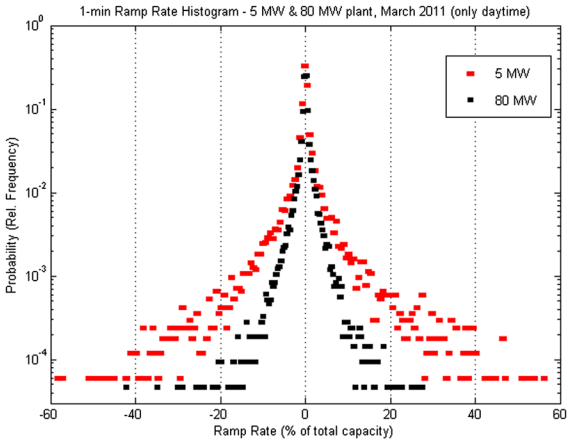

Figure 9. Ramp rate histograms for the 5 MW and 80 MW plant, March 2011. The horizontal groupings that are apparent in the regions of high ramp rates indicate the number of occurrences, with the lowest representing one occurrence, then two, three, and so on.

($RR_{60s,max}$) was 0.47 p.u. or 38 MW/min. Although we do not know what the cloud velocity was at that time, this value is in line with the theoretical maximum observed in Figure 2.

As would be expected, we observe that the curves shift to the right with increasing DARR category. Still, the highest observed ramp is not from a "Category 5" day; in this case, it happened on a "Category 4" day. This is because the DARR summarizes overall variability only for a single day and does not account for shorter times with marked variability. The DARR therefore gives a probabilistic indication of what ramps can be expected on that particular day. Our next logical step was to plot another cumulative probability distribution, now with the plant output data from all sites. The results, obtained on the most variable days (Category 5: $DARR_{min} \geq 33$ p.u.) are displayed in Figure 12.

During "Category 5" days, the benefit of geographic dispersion becomes apparent especially for plants with a capacity beyond 30 MW. Observed maximum ramp rates from the 80 and 48 MW_{AC} plants are ~0.4 and ~0.5 p.u., respectively, with the first showing only two occurrences of ramps above 0.34 p.u. In Figure 13, $RR_{60s,max}$ are plotted as a function of the plants' shortest sides, L. According to the basic model introduced earlier, the $RR_{60s,max}$ for plants with $L = 3000$ m (> 150 MW) would generate ramps of up to ~0.2 p.u. at 25 m/s cloud velocity, further decreasing as L increases. For now, we set two arbitrary cloud velocities to show the effect of L on $RR_{60s,max}$ but a follow-up study is needed with cloud velocity data to validate the effect of V and L together.

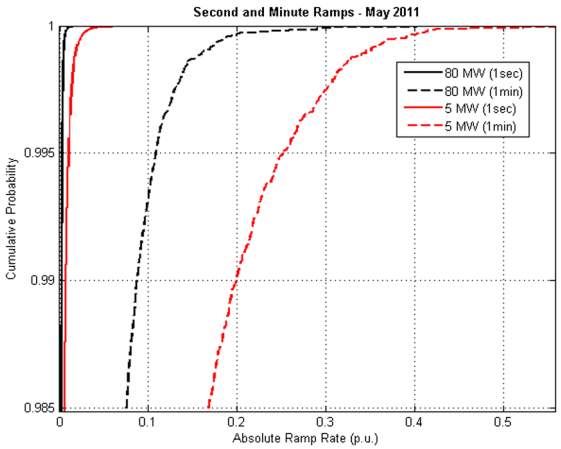

Figure 10. Second and minute ramps observed from a 5 and 80 MW plant in Ontario, Canada.

8. CONCLUSIONS

The variability of utility-scale solar PV plants is a cause of concern for grid operators as numerous large-scale (>250 MW) PV plants are coming online. More specifically, grid operators are concerned about the very short-term ramp rates exhibited by PV plants.

Generally, it is believed that the short-term ramp rates become attenuated as the size of the plant increases. At the time of writing, the effect of geographic dispersion on the observed ramp rates has been studied primarily with several small PV systems or point-irradiance sensors dispersed over a large area. This smoothing effect was not previously validated for fixed-tilt multi-megawatt plants. In this study, we demonstrated this phenomenon on the basis of actual 1 min-averaged power output data from six PV plants ranging in size from 5 to 80 MW located in the southwest of the USA and southeast Canada.

The maximum ramp rates observed in this study are typically higher than those found by the studies shown in Table I (0.7 p.u. for the 5 MW plant versus 0.5 p.u. for a 4.6 MW plant published by Hansen [16]). This is likely due to the fact that the data set used here covers more days

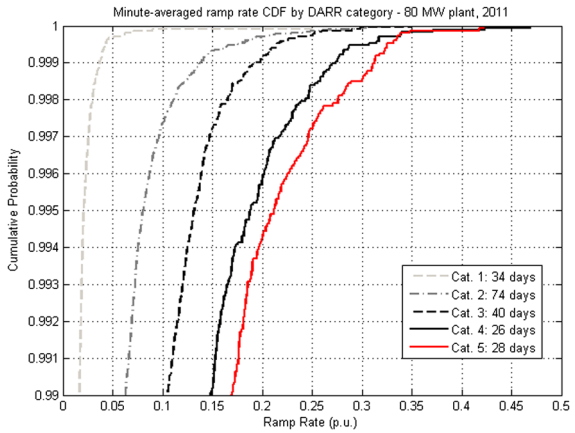

Figure 11. Using the DARR categorization based on a single irradiance sensor, the ramp rates at the 80 MW plant are visualized with cumulative distribution functions for each category of day in the period January–June 2011.

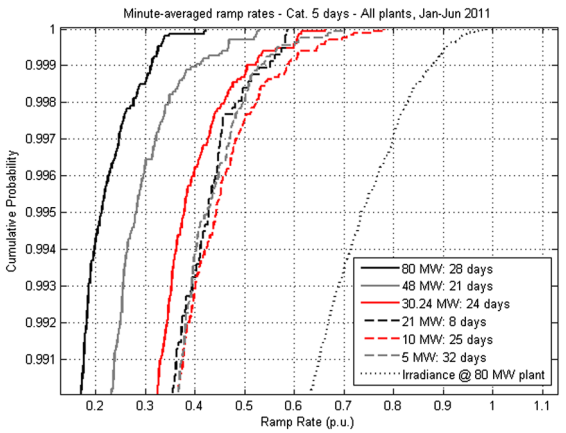

Figure 12. Cumulative probability function of observed ramp rates across all plants in the portfolio for "Category 5" days ($DARR > 33$) in January–June of 2011. For reference, we show the curve of ramp rates observed from a point irradiance sensor at the 80 MW plant.

DOI: 10.1002/pip

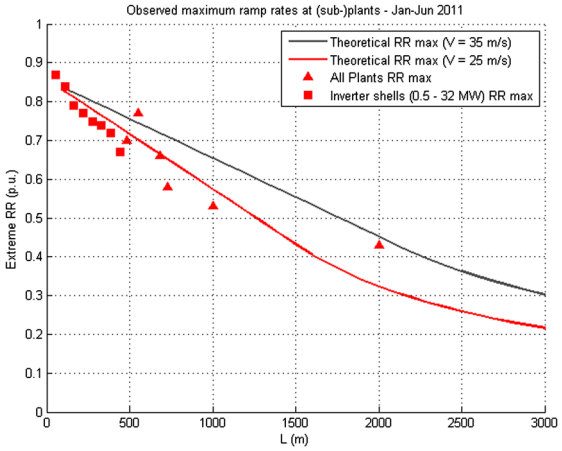

Figure 13. Observed maximum ramp rates for different sized plants and sub-plants using the inverter shells method and time averaging period = 60s. The two lines represent the theoretical maxima from Figure 2, for $V = 35$ and 25 m/s.

than others, which makes it more probable that high ramp rates are included in the data.

We show a reduction in observed $RR_{60s,3\sigma}$ (1 min normalized absolute ramp rates, 3σ probability) from 0.47 to 0.25 p.u. for the 5 MW plant versus the 80 MW plant on most variable "Category 5" days.

Employing data from the 48 MW plant, we demonstrated that irradiance sensor data can be used for estimating minute-averaged extreme ramp rates ($RR_{60s,max}$) provided that multiple sensors are adequately distributed over the virtual plant and that the data are properly clipped to account for limited inverter output. Extreme ramp rates were estimated from clipped data with an error $<3\%$ between $RR_{60s,3\sigma}$ and $RR_{60s,max}$ compared with a 10% error for unclipped data.

The effect of geographic dispersion was demonstrated using the "inverter shells method," wherein variability was assessed in each step of a plant growing from 0.5 to 32 MW. Extreme ramp rates ($RR_{60s,max}$) decreased from 0.87 to 0.67 p.u., respectively, whereas $RR_{60s,3\sigma}$ decreased more rapidly with L from 0.56 to 0.24 p.u., which is in line with the probabilistic theory of wind/cloud speed occurrence and shortest plant side L

To support comparisons of fluctuations in power output across multiple sites with different weather conditions, we introduced the DARR as a metric to summarize daily variability from a single irradiance sensor. Five categories were defined, ranging from stable days (Category 1) to highly variable days (Category 5). All plant days in the portfolio were distributed across these categories, and ramp rates observed in Category 5 days were compared for all plants. It was shown that absolute ramp rates decrease as plant size increases. A simple model was used to estimate extreme ramp rates; our results were shown to give a good indication of the highest observed ramps. Further efforts will be put into validation of the model with data on cloud velocity and a distribution of cloud sizes.

9. FURTHER RESEARCH NEEDS

In this study, we used a time scale of 1 min as the period over which power output was averaged. However, a series of power-output data were found across the plant portfolio that contained sequences of alternating ramp rate signs (Figure 6), implying that sub-minute fluctuations could have occurred. Therefore, the ramp that was recorded could have been higher or lower if the time-averaging period started 30 s earlier than it did. A follow-up study using a higher time resolution could give insight into what time scale is necessary to capture all output fluctuations; this is likely to depend heavily on the plant size and weather conditions.

It is evident that the DARR, as a variability summarizing metric, does not capture the individual ramp rates that occur during the day. Therefore, it can only give a potential measure to determine the level of spinning reserves capacity necessary to balance ramping. Also, the metric can perhaps be adjusted for length of day and peak irradiance, as winter days are shorter than summer days and reach lower peak irradiance under clear sky conditions. Further research is needed using day-ahead forecasting measures to assess what DARR category is expected and during what time of the day variability is expected. Also, investigations are needed to identify the ramps as a function of observed cloud size, opacity, and velocity. With this information, one can validate and expand the theory introduced here for estimating extreme ramp rates as a function of cloud velocity and plant size. Finally, it would be interesting to analyze how the ramps of other PV technologies would differ from that of CdTe, considering the differences in spectral response and efficiency.

ACKNOWLEDGEMENTS

Special thanks to First Solar for making data available to this study and for their summer internship program. Also, the authors would like to acknowledge John Bellacicco and their fellow research group members at the Center for Life-Cycle Analysis (especially Daniel Wolf) for the valuable inputs and brainstorm sessions.

REFERENCES

1. Danish Energy Agency. *Energy Statistics 2009. Energy*. Copenhagen. 2010. Retrieved from http://www.ens.dk/en-US/Info/FactsAndFigures/Energy_statistics_and_indicators/Annual Statistics/Documents/Energi Statistics 2009.pdf, Accessed: 10 November 2011.
2. German Energy Ministry. *Erneuerbare Energien 2010. Vierteljahrshefte zur Wirtschaftsforschung* 2011; **76**. DOI: 10.3790/vjh.76.1.35
3. Ekman CK. On the synergy between large electric vehicle fleet and high wind penetration—an analysis of the Danish case. *Renewable Energy* 2010; **36**(2):

546–553. Elsevier Ltd. DOI: 10.1016/j.renene.2010.08.001

4. Lew D, Miller N, Clark K, Jordan G. Impact of high solar penetration in the western interconnection. *National Renewable Energy Agency*, December 2010. Retrieved from: http://www.nrel.gov/wind/systemsintegration/pdfs/2010/lew_solar_impact_western.pdf
5. Nikolakakis T, Fthenakis V. The optimum mix of electricity from wind- and solar-sources in conventional power systems: evaluating the case for New York State. *Energy Policy* 2011; 1–9. Elsevier. DOI: 10.1016/j.enpol.2011.05.052
6. Ummels BC, Gibescu M, Pelgrum E, Kling WL, Brand AJ. Impacts of wind power on thermal generation unit commitment and dispatch. *IEEE Transactions on Energy Conversion* 2007; **22**(1): 44–51. DOI: 10.1109/TEC.2006.889616
7. Denholm P, Margolis RM. Evaluating the limits of solar photovoltaics (PV) in electric power systems utilizing energy storage and other enabling technologies. *Energy Policy* 2007; **35**(9): 4424–4433. Elsevier. DOI: 10.1016/j.enpol.2007.03.004
8. Red Electrica De Espana. Red Electrica De Espana. 2010. Retrieved from http://www.ree.es/
9. Gansler R, Klein S, Beckman W. Investigation of minute solar radiation data. *Solar Energy* 1995; **55**(1): 21–27. Elsevier. Retrieved from http://linkinghub.elsevier.com/retrieve/pii/0038092X9500025M
10. Jurado M. Statistical distribution of the clearness index with radiation data integrated over five minute intervals. *Solar Energy* 1995; **55**(6): 469–473. DOI: 10.1016/0038-092X(95)00067-2
11. Suehrcke H, McCormick P. Solar radiation utilizability. *Solar energy* 2010; **43**(6): 339–345. Elsevier. Retrieved from http://linkinghub.elsevier.com/retrieve/pii/0038092X89901047
12. Mills A, Wiser R. Implications of wide-area geographic diversity for short-term variability of solar power. *Berkeley Lab*, September 2010. Retrieved from http://eetd.lbl.gov/ea/ems/reports/lbnl-3884e.pdf
13. Hoff TE, Perez R. Quantifying PV power output variability. *Solar Energy* 2010; **84**(10): 1782–1793. Elsevier Ltd. DOI: 10.1016/j.solener.2010.07.003
14. Stein JS. PV output variability, characterization and modeling. *Integration of Renewable and Distributed Energy Resources*. Albuquerque, NM: Sandia National Laboratories. 2010.
15. Wiemken E, Beyer HG, Heydenreich W, Kiefer K. Power characteristics of PV ensembles: experiences from the combined power production of 100 grid connected PV systems distributed over the area of Germany. *Solar Energy* 2001; **70**(6): 513–518. DOI: 10.1016/S0038-092X(00)00146-8
16. Hansen T. *Utility solar generation valuation methods*. *Chemical record (New York, N.Y.)* 2011; **11**. Tucson, AZ. DOI: 10.1002/tcr.201190008
17. Curtright AE, Apt J. The character of power output from utility-scale photovoltaic systems. *Power* (September 2007) 2008; 241–247. DOI: 10.1002/pip
18. Kankiewicz A, Sengupta M, Moon D. Observed impacts of transient clouds on utility-scale PV fields. *Solar* 2010 *Conference Proceedings* (Vol. 2009). American Solar Energy Society first. 2010.
19. Lenox C. Variability in a large-scale PV installation. *Utility-scale PV Variability Workshop*. Cedar Rapids, IA: NREL. 2009.
20. Blatchford,J. Telephone interview James Blatchford. 2011; interview date: 4 August 2011.
21. Mills A, Ahlstrom M, Brower M, Ellis A, George R, Hoff T, Kroposki B, et al. Dark shadows. *IEEE Power and Energy Magazine* June 2011; 33–41. Retrieved from http://ieeexplore.ieee.org/xpls/abs_all.jsp?arnumber=5753337
22. Perez R, Hoff TE, Schlemmer J, Kivalov S, Hemker KJ. *Short-Term Irradiance Variability—Station Pair Correlation as a Function of Distance*. American Solar Energy Society Annual Conference: Raleigh, NC, 2011.
23. Murata A, Yamaguchi H, Otani K. A method of estimating the output fluctuation of many photovoltaic power generation systems dispersed in a wide area. *Electrical Engineering in Japan* 2009; **166**(4): 9–19. DOI: 10.1002/eej.20723
24. Horváth Á, Davies R. Feasibility and error analysis of cloud motion wind extraction from near-simultaneous multiangle MISR measurements. *Journal of Atmospheric and Oceanic Technology* 2001; **18**(4): 591–608. Retrieved from http://journals.ametsoc.org/doi/abs/10.1175/1520-0426 (2001)018%3C0591%3AFAEAOC%3E2.0.CO%3B2
25. Plank VG. The size distribution of cumulus clouds in representative Florida populations. *Journal of Applied Meteorology* 1969; **8**: 46–67. Retrieved from http://adsabs.harvard.edu/abs/1969JApMe. . .8. . .46P
26. Lave M, Kleissl J. Testing a wavelet-based variability model (WVM) for solar PV power plants. *Power and Energy Society*. Conference Proceedings, 2011.
27. Kawasaki N, Oozeki T, Otani K, Kurokawa K. An evaluation method of the fluctuation characteristics of photovoltaic systems by using frequency analysis. *Solar Energy Materials and Solar Cells* 2006; **90**(18–19): 3356–3363. DOI: 10.1016/j.solmat.2006.02.034
28. Lave M, Kleissl J. Solar variability of four sites across the state of Colorado. *Renewable Energy* 2010; **35**(12): 2867–2873. Elsevier Ltd. DOI: 10.1016/j.renene.2010.05.013